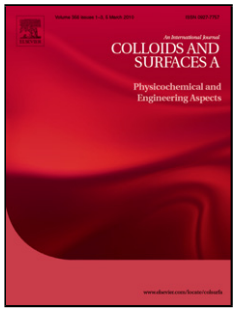

Title: Zeta potential in sandpacks: effect of temperature, electrolyte pH, ionic strength and divalent cations

Authors: Jan Vinogradov, Matthew D. Jackson, Manuel Chamerois

PII: S0927-7757(18)30416-3
DOI: https://doi.org/10.1016/j.colsurfa.2018.05.048
Reference: COLSUA 22516

To appear in: *Colloids and Surfaces A: Physicochem. Eng. Aspects*

Received date: 9-2-2018
Revised date: 16-5-2018
Accepted date: 16-5-2018

Please cite this article as: Vinogradov J, Jackson MD, Chamerois M, Zeta potential in sandpacks: effect of temperature, electrolyte pH, ionic strength and divalent cations, *Colloids and Surfaces A: Physicochemical and Engineering Aspects* (2018), https://doi.org/10.1016/j.colsurfa.2018.05.048

Zeta potential in sandpacks: effect of temperature, electrolyte pH, ionic strength and divalent cations.

Authors

Jan Vinogradov[1,2], Matthew D. Jackson[1], Manuel Chamerois[3]

Affiliation

[1]Department of Earth Science and Engineering, Imperial College London, UK.

[2]Now at the School of Engineering, University of Aberdeen, UK.

[3]TOTAL Research, Pau, France.

Graphical abstract

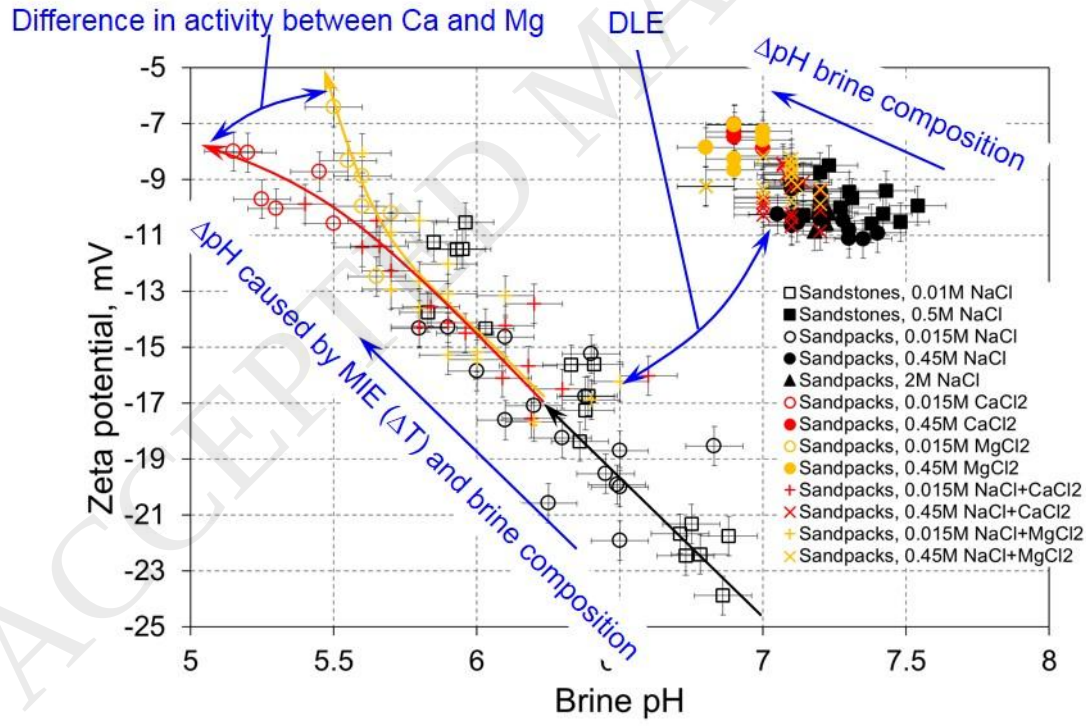

Abstract

Rocks in many subsurface settings are at elevated temperature and are saturated with brines of high ionic strength (high salinity) containing divalent ions. Yet most laboratory measurements

of zeta potential in earth materials are obtained at room temperature using simple monovalent electrolytes at low ionic strength. Consequently, the zeta potential at conditions relevant to many subsurface settings is not known. We report experimental measurements of the temperature dependence of the zeta potential in well characterised, natural quartz sandpacks over the temperature range 23-120°C saturated with electrolytes containing divalent ions at a range of concentrations relevant to natural systems. We find that the key control on zeta potential in these unbuffered experiments is pH, which varies in response to temperature and electrolyte composition. The zeta potential is negative irrespective of sample or electrolyte, but its magnitude is strongly correlated to pH, which varies both with temperature and the concentration of divalent ions. The pH decreases with increasing temperature at low ionic strength, but is independent of temperature at high ionic strength. The pH is also typically lower in the presence of divalent ions, irrespective of the total ionic strength. The zeta potential increases in magnitude with increasing pH. Different relationships between zeta potential, temperature and concentration of divalent ions could be obtained in buffered experiments where the pH is fixed at a given value.

1. Introduction

The zeta potential is a measure of the electrical potential at mineral surfaces in water-saturated rocks. Its magnitude and polarity control the electrostatic interactions between the mineral surfaces and polar or ionic species present in both aqueous and non-aqueous phase fluids and the magnitude and polarity of the self-potential (SP) arising from electrokinetic and charge exclusion processes (e.g. *Jouniaux and Pozzi*, 1995; *Revil*, 1999; *Maineult et al.*, 2004; *Glover et al.*, 2012; *Leinov and Jackson*, 2014).

In many subsurface settings, including geothermal fields (*Corwin and Hoover*, 1979; *Fitterman and Corwin*, 1982; *Ishido et al*., 1989; *Revil and Pezard*, 1998; *Darnet et al*., 2004;

Jardani et al., 2008), deep saline aquifers (*Moore et al*., 2004; *Ishido et al*., 2013), hydrocarbon reservoirs (*Gulamali et al*., 2011; *Saunders et al*., 2012), volcanoes (*Aubert and Atangana*, 1996; *Michel and Zlotnicki*, 1998; *Jouniaux et al*., 2000; *Revil et al*., 2011) and during seismoelectric exploration (*Revil and Mahardika*, 2013; *Jouniaux and Zyserman*, 2016), the rocks are at elevated temperature and are saturated with brines of high ionic strength (high salinity) containing divalent ions such as Ca^{2+}, Mg^{2+} and SO_4^{2-}. Yet most laboratory measurements of zeta potential in earth materials are obtained at room temperature using simple monovalent electrolytes at low ionic strength (see *Walker et al*., 2014 for a compilation). Previous studies have investigated high ionic strength but monovalent electrolytes (e.g. *Jaafar et al.*, 2009; *Vinogradov et al.*, 2010; *Walker and Glover*, 2018), elevated temperature but monovalent electrolytes (e.g. *Vinogradov and Jackson*, 2015) and electrolytes containing divalent ions but at ambient temperature (e.g. *Coreño et al*., 2001; *Lorne et al*., 1999 *Mammen et al*., 1997; *Pierre et al*., 1990; *Thanh and Sprik*, 2016). Consequently, the zeta potential at conditions relevant to many subsurface settings is not known.

In many natural and engineered earth processes, brine of one composition is replaced by brine of a different composition and/or ionic strength. Such displacements are observed when saline water or a saline tracer invades a freshwater zone (e.g. *Boleve et al.*, 2011; *Jougnot et al.*, 2015; *MacAllister et al*., 2016) and *vice-versa* (e.g. *Appelo*, 1994; *Valocchi et al.*, 1981) and during oil recovery by controlled salinity waterflooding (CSW) (e.g. *Jackson et al.*, 2016a). Yet the effect of compositional changes, or the history of compositional changes, on the zeta potential of earth materials at the conditions of elevated temperature and/or ionic strength relevant to subsurface systems is also not known.

The aim of this study is to determine the temperature dependence of the zeta potential in pure, natural quartz sandpacks over the temperature range 23-120°C, saturated with NaCl

electrolytes containing the divalent ions Ca^{2+} and/or Mg^{2+} at 0.015M (comparable to potable water; 1 M = 1 mol dm^{-3}), 0.45M (comparable to seawater) and 2M (comparable to formation brines in deep saline aquifers) ionic strength. We use well characterised, natural quartz sandpacks as analogues for natural sandstones, arguing that a thorough understanding of these simpler analogue materials is essential prior to investigating sandstones and the additional complexities associated with multiple mineral phases.

2. Materials and method

2.1. Sandpack preparation and initial characterisation

The zeta potential was determined using the streaming potential method (e.g. *Delgado et al.*, 2007). The streaming potential and, from this, the zeta potential was determined using the methodology of *Vinogradov et al*. (2010) and *Vinogradov and Jackson* (2015) implemented in a multi-sample setup developed as part of this study (Figure 1). The streaming potential was measured on packed samples of Ottawa and Fontainebleau sand, both characterised by >99% quartz content. The sand was poured into an FEP heat shrink sleeve with internal diameter of 38mm which matches that of the core holders. To ensure full water saturation (S_w=1), the sandpacks were prepared by pouring the sand into the sleeve partially filled with the electrolyte of interest until the required length of pack was achieved. To ensure consistent properties, intensive tapping of the sleeve walls was used and axial pressure of c. 800kPa was applied onto the end-caps after the pack was sealed.

Sandpack mass and volume (by water displacement) were measured to calculate the sand grain density, and mass balance between empty and fully assembled core holders was used to determine the porosity. The electrical conductivity of each pack was measured using the methodology reported by *Vinogradov et al*. (2010). The absolute liquid permeability (k) was measured during coreflooding experiments and the formation factor (F) was measured at

ambient temperature (21°C). The sandpack preparation method provided consistent results for over 30 sandpacks used in the experiments, with the average petrophysical properties of the sandpacks shown in Table 1. Note that the uncertainty of the properties represents the repeatability across different packs.

2.2. Electrolytes

The electrolytes used in this study were solutions of reagent-grade NaCl, $CaCl_2 \cdot 2H_2O$, $MgCl_2 \cdot 6H_2O$ (Sigma Aldrich UK) in deionised water (electrical conductivity <1μS/cm). The electrolytes were prepared in volumetric flasks open to atmospheric CO_2; the electrolyte pH and electrical conductivity was measured at regular intervals and chemical equilibrium was assumed to have established when these properties remained unchanged and constant for over 3 hours. The electrolytes used in our experiments and their properties are given in Table 2. After the initial equilibration, the electrolyte of interest was used to saturate the sandpack. Once loaded into the core holder, the experimental setup ensures that the sample and electrolytes are isolated from atmospheric CO_2 during measurements of streaming potential.

2.3. Experimental methodology

Prior to carrying out the streaming potential measurements, chemical equilibrium between samples and electrolytes was established at a given temperature following the procedure described by *Vinogradov and Jackson* (2015). There was no attempt to fix the pH at a given value; the pH in a given experiment reflects the equilibrium obtained for a given electrolyte, sand and temperature. To measure the streaming potential coupling coefficient (C_{sp}) we used the paired-stabilization (PS) method described by *Vinogradov and Jackson* (2011). The zeta

potential was calculated from the streaming potential coupling coefficient using the modified Helmholtz-Smoluchowski equation (e.g. e.g. *Jouniaux and Pozzi*, 1995; *Glover*, 2015).

$$C_{sp} = \frac{\Delta V}{\Delta P} = \frac{\varepsilon \zeta}{\mu \sigma_r F} \qquad \text{Eq. 1}$$

Here μ is the dynamic viscosity of the electrolyte, ε is the electrical permittivity of the electrolyte, σ_r is the electrical conductivity of the saturated samples (measured following the procedure described in detail by *Vinogradov et al*., (2010)), and F is the intrinsic formation factor of the samples. The intrinsic formation factor is defined as the ratio between the electrical conductivity of the electrolyte and the electrical conductivity of the sample saturated with the same electrolyte when the surface conductivity is negligible, i.e. at high ionic strength. The intrinsic formation factor was measured at ambient temperature following the procedure described by *Vinogradov et al*., [2010]. We obtained μ and ε as a function of temperature and ionic strength using the approach of *Saunders et al*. (2012) (see his Appendix A). The apparent (measured) zeta potential in streaming potential experiments may significantly differ from the true one if the electrical double layers (EDL) from the opposite pore walls overlap [*Datta et al*., 2010; *Leinov and Jackson*, 2014]. However, in the experiments reported here, the EDL thickness is more than three orders of magnitude smaller than the pore radius of the sandpacks (of order 10s μm), so no correction is required.

At the end of each PS experiment, two electrolyte samples were collected using sealed sampling tubes: one sample was used for the measurements of electrolyte electrical conductivity and pH; the second electrolyte sample was allowed to cool down to ambient temperature and a repeat measurement of electrolyte pH and a complete chemical analysis (using a Metrohm 930 Compact ion chromatographer) was carried out for comparison.

2.4. Design of experiments

To determine the effect of temperature, ionic strength and divalent ions on the zeta potential of the sandpacks, four distinct sets of experiments were conducted:

1. Effect of Na concentration and temperature. The aim of these experiments was to determine whether the sandpacks show similar temperature- and concentration-dependent behaviour in a simple monovalent electrolyte as the natural sandstones investigated previously by *Vinogradov et al*. (2010) and *Vinogradov and Jackson* (2015). Zeta potential was measured for 0.015M, 0.45M and 2M NaCl electrolyte at temperature up to 120ºC (NaCl electrolytes in Table 2).
2. Effect of Ca and Mg concentration and temperature. The aim of these experiments was to determine the impact on the zeta potential of individual divalent ions that are abundant in natural brines. The impact of these ions at concentrations relevant to natural brines has not been determined previously (see *Thanh and Sprik* (2016) for data at low ionic strength and laboratory temperature). Zeta potential was measured for pure $CaCl_2$ and $MgCl_2$ electrolytes at 0.015M and 0.45M ionic strength and temperature up to 120ºC ($CaCl_2$ and $MgCl_2$ electrolytes in Table 2).
3. Effect of temperature and Ca or Mg concentration in mixed electrolytes containing Na. The aim of these experiments was to determine the impact of Ca and Mg on zeta potential in electrolytes containing Na and one of these divalent ions in a 9:1 proportion relevant to natural brines. These mixed electrolytes (NaCl:$CaCl_2$ and NaCl:$MgCl_2$ in the ratio 9:1 TDS; NaCl-$CaCl_2$ and NaCl-$MgCl_2$ electrolytes in Table 2) have been used in previous experiments (e.g. *Cissokho et al*., 2010). The effect of saturation history of these simple single and mixed electrolytes was also tested (Table 3).
4. Effect of saturation history using variable electrolyte concentrations. The aim of these experiments was to determine the change in zeta potential in response to changes in brine

composition relevant to CSW. A number of different saturation histories were investigated (see Table 4).

3. Results

We begin by briefly reporting the results of chemical analysis of the electrolytes used in the experiments, with analysis conducted on a given electrolyte before it contacted the sandpack, and at the end of the streaming potential measurements. Analysis for anions (Cl^-) and cations (Na^+; Ca^{2+}; Mg^{2+}) in the effluent electrolytes showed no measurable change in concentration for all electrolytes and temperature conditions used in the experiments. This is an important result that will be referred to later in the paper. Note also that all measured zeta potentials in the experiments reported here were negative.

3.1. NaCl concentration and temperature

Figure 2 shows the variation of zeta potential with ionic strength in sandstones at laboratory temperature (data compiled in *Vinogradov et al*. (2010) with the new data obtained here on Fontainebleau and Ottawa sand). The sandpack data follow the same trend as natural sandstones, most notably in that the zeta potential is the same within experimental uncertainty for the ionic strengths of 0.45M and 2M. Values of the measured zeta potential agree well with previously published results and are in line with the conclusion that the zeta potential becomes independent of ionic strength for ionic strength >0.45M, that was first postulated by *Jaafar et al*., (2009) and *Vinogradov et al*., (2010) and later confirmed by *Walker et al*. (2014) and *Walker and Glover* (2018). *Vinogradov et al*. (2010) argued that the decoupling of zeta potential at high ionic strength reflects a change in behavior of the ion density in the diffuse

part of the electrical double layer: at low ionic strength, the behavior is Boltzmann-like, whereas at high ionic strength the density is controlled by ion-ion interactions.

Figure 3 shows the temperature dependence of zeta potential in Ottawa and Fontainebleau sand at low (0.015M; Figure 3a) and moderate- to high- ionic strength (0.45M and 2M; Figure 3b). The data for each sand type are the same within experimental error. Also shown for comparison are data from natural sandstones obtained by *Vinogradov and Jackson* (2015). The sandpack data follow the same trend as the natural sandstones: at low ionic strength, the negative zeta potential decreases in magnitude with increasing temperature, while at moderate to high ionic strength, the zeta potential is independent of temperature. The temperature dependence of the zeta potential at low ionic strength is consistent with the model of *Revil et al*. (1999) if the empirical temperature dependence of pH is accounted for (Figure 4); the constant value at moderate to high ionic strength is consistent with the model of *Saunders et al*. (2012). We extrapolate the empirical correlation between pH and the temperature beyond the range of directly measured values (>80^{o}C) as a first order hypothesis (Fig.4). The correlation provides a good match for the temperature dependence of the zeta potential using the model of *Revil et al*., (1999) in the low salinity domain. However, to confirm the correlation at high temperature requires a modification of the experimental setup to allow *in-situ* measurements of the electrolyte pH.

3.2. Ca and Mg concentration and temperature

At low ionic strength, there is a weaker temperature dependence of the zeta potential in both $CaCl_2$ and $MgCl_2$ electrolytes than in NaCl electrolyte, with the zeta potential decreasing in magnitude (becoming less negative) with increasing temperature. The temperature sensitivity of $MgCl_2$ is greater than $CaCl_2$. For example, in Ottawa sand, the zeta potential decreased from c. -12.5mV at laboratory temperature to c. -7.8mV at 120^{o}C (a change of 4.7mV) in $MgCl_2$,

but from c. -10.8mV to c. -9.2mV in $CaCl_2$ (a change of 1.6mV). The Ottawa sand in both $CaCl_2$ and $MgCl_2$ electrolytes consistently yielded a more negative zeta potential (larger in magnitude) than the Fontainebleau sand. At moderate ionic strength, the zeta potential remained constant within experimental error.

There is no model currently available to describe the temperature dependence of the zeta potential in the moderate to high ionic strength 2:1 electrolytes used here. The model of *Revil et al*. (1999) is valid only for 1:1 electrolytes, and a recent model reported by *Thanh and Sprik* (2016) is valid only for symmetric electrolytes. The model of *Datta et al*. (2009) is valid for asymmetric and mixed electrolytes at low concentration and ambient temperature, and indicates that the presence of Ca cations results in a less positive (smaller magnitude) zeta potential compared to electrolytes containing only Na or Mg cations, consistent with the results obtained here at similar conditions (see Figure 5a; data at 20ºC). All of the models mentioned above are restricted to Boltzmann distribution of ions in the diffuse part of the electrical double layer, which breaks down at moderate and high salinity.

The less positive (smaller magnitude) zeta potential in $CaCl_2$ and $MgCl_2$ electrolytes compared to NaCl electrolyte is consistent with the lower observed pH, and the weaker temperature dependence of the zeta potential is consistent with the weaker temperature dependence of the pH (Figure 6a). Moreover, the lack of temperature dependence of the zeta potential at moderate to high ionic strength is consistent with the lack of temperature dependence of pH (Figure 6b). We consider further the relationship between zeta potential and pH in the Discussion.

3.3. Ca or Mg concentration in mixed electrolytes containing Na

Figure 7 shows the temperature dependence of zeta potential in Ottawa and Fontainebleau saturated with pure and mixed $CaCl_2$ electrolytes at low (0.015M; Figure 7a) and moderate

(0.45M; Figure 7b) ionic strength (see Table 3 for a summary of the flooding sequence of electrolytes). Also shown for comparison are the data for the corresponding NaCl electrolyte shown in Figure 4. Note again that the ionic strength in each plot is the same regardless of the ionic species in solution, so differences in the temperature-dependence of the zeta potential in a given plot reflect only differences in the dominant ion type and history, rather than changes in ionic strength.

At low ionic strength, the pure $CaCl_2$ electrolyte shows the least negative (smallest magnitude) zeta potential and the pure NaCl electrolyte shows the most negative (largest magnitude) zeta potential. The mixed NaCl-$CaCl_2$ electrolyte yields values of zeta potential that lie between these two limits, and the value of zeta potential depends upon whether the sample was initially saturated with $CaCl_2$ or NaCl electrolyte (shown in brackets). The zeta potential is more negative (larger in magnitude) in samples initially saturated with pure NaCl electrolyte than in samples initially saturated with pure $CaCl_2$ electrolyte. The temperature dependence of the zeta potential is also least significant for the pure $CaCl_2$ electrolyte and most significant for the pure NaCl electrolyte, and is more significant for the mixed electrolyte in samples initially saturated with pure NaCl electrolyte than in samples initially saturated with pure $CaCl_2$ electrolyte.

At moderate ionic strength, the zeta potential values for the mixed NaCl-$CaCl_2$ electrolyte again lie between the maximum and minimum limits obtained from the pure NaCl and $CaCl_2$ electrolytes respectively, with more negative (larger in magnitude) values when the samples are initially saturated with NaCl electrolyte and less negative (smaller in magnitude) values when the samples are initially saturated with pure $CaCl_2$ electrolyte. The zeta potential shows no variation with temperature irrespective of the electrolyte composition.

Figure 8 shows the temperature dependence of zeta potential in Ottawa and Fontainebleau saturated with pure and mixed $MgCl_2$ electrolytes at low (0.015M; Figure 8a) and moderate

(0.45M; Figure 8b) ionic strength. Also shown for comparison are the data for the corresponding NaCl electrolyte shown in Figure 3. The trends observed are similar to those obtained for the Ca electrolytes shown in Figure 7. The most significant difference is that the temperature dependence of the zeta potential at low ionic strength is more pronounced in the Mg electrolytes than in the Ca electrolytes, as discussed in the previous section. Note that in all cases, the zeta potential behavior depends on the composition history, as it is different for a given multivalent electrolyte if the sample was initially saturated with NaCl electrolyte.

3.4. Effect of electrolyte composition and dilution relevant to CSW

The process of CSW involves changing the injection brine composition during oil recovery in a way that modifies the ionic strength and/or concentration of divalent ions and so will impact on the zeta potential (see *Jackson et al.,* 2016b for an overview). This final set of experiments tested the effect of electrolyte composition and dilution on the zeta potential of the sandpacks.

Figure 9 shows the change in zeta potential as various initial 2M electrolytes are changed for electrolytes with lower ionic strength at high (120ºC; dashed lines) and low (23ºC; solid lines) temperature. Intermediate temperatures were also tested and yield behavior that lies between the solid and dashed lines. In some experiments, the composition was also changed. Straight lines with no change in slope at 0.45M ionic strength represent 'secondary' waterflooding in which the initial 2M electrolyte is replaced by 0.015M electrolyte; lines with a change in slope at 0.45M ionic strength represent 'tertiary' waterflooding in which the initial 2M electrolyte is replaced by 0.45M electrolyte and then 0.015M electrolyte. The electrolyte compositions at each step are shown in the figure caption and correspond to those shown in Tables 2 and 4.

Reducing ionic strength from 2M to 0.45M yields no change in zeta potential if the initial electrolyte contains divalent ions, or if neither the initial nor dilute electrolyte contains divalent

ions (see curves for FMB → SW and Na → Na). However, if the initial 2M electrolyte only contains monovalent (Na) ions and the dilute electrolyte at 0.45M contains divalent (Ca or Mg) ions then the zeta potential becomes less negative, yielding a positive change in zeta potential (see curves for Na → Ca and Na → Mg). However, reducing the ionic strength to 0.015M always yields a more negative zeta potential irrespective of the presence of divalent ions.

The largest (negative) change in zeta potential occurs when FMB electrolyte of either composition is directly replaced by SW/30 electrolyte (FMB → SW/30) in a 'secondary' waterflood at 23ºC. However, the equivalent 'tertiary' waterflood (FMB → SW → SW/30) and simple dilution of Na electrolyte (Na → Na → Na) yields a similar change. The smallest change in zeta potential occurs when 2M NaCl is replaced by Ca or Mg electrolyte in a 'tertiary' waterflood at elevated temperature (see dashed curves for Na → Ca → Ca and Na → Mg → Mg). In general, negative changes in zeta potential are suppressed at elevated temperature, although the positive change observed when Na is replaced by Ca or Mg is largest at elevated temperature. Both Ottawa and Fontainebleau samples show similar behavior.

4. Discussion

The key control on zeta potential in these unbuffered experiments is pH, which varies in response to temperature and brine composition. We observed a negative zeta potential irrespective of sample or electrolyte, the magnitude of which is strongly correlated to pH, where the pH varies either because the temperature varies, or because the concentration of divalent ions changes (Figure 11). The data form two distinct trends corresponding to low (0.015M) and high (0.45 and 2M) ionic strength electrolytes. The pH generally decreased with increasing temperature at low ionic strength, but was independent of temperature at high ionic strength (see *Vinogradov and Jackson* (2015) for similar results on natural sandstones). The pH was also typically lower in the presence of divalent ions, irrespective of the total ionic

strength. It is possible that a different relationship between zeta potential, temperature and concentration of divalent ions would be obtained in buffered experiments where the pH is fixed at a given value by addition of controlled amounts of acid or base.

4.1 Effect of pH, temperature and salt species

The initial electrolyte pH at ambient temperature was dictated by the concentration of H^+ in equilibrium with the salt species of interest and atmospheric CO_2, recalling that the electrolytes were prepared by adding salts to de-ionized water in open flasks. However, during heating and cooling, the electrolytes were in the closed system of the experimental setup (Fig. 1). In the low ionic strength electrolytes, the pH decreased in magnitude with increasing temperature, but any temperature dependence of the pH was too small to resolve in the moderate and high ionic strength electrolytes (see Fig. 4 for NaCl data and Fig. 6 for $CaCl_2$ and $MgCl_2$ data).

The temperature dependence of pH can be interpreted, at least in part, in terms of enhanced dissociation of the water molecules (*Millero et al*., 2009). This process is reversible with respect to temperature, confirmed here in separate experiments in which samples of electrolyte were heated and cooled in a closed system without contact with sand. However, when the samples were in contact with sand, the temperature dependent change in pH was irreversible (Figure 12; see also *Vinogradov and Jackson*, 2015). *Vinogradov and Jackson* (2015) hypothesized that, in addition to the dissociation of water molecules, some ion exchange occurs with the mineral surfaces, with protons from the silanol group being replaced by salt ions from the electrolyte. However, preliminary surface complexation modelling has failed to reproduce the irreversible pH change, because the surface reactions are assumed to be reversible. Further work is required to understand and explain the irreversible changes in pH observed here in sandpacks, and by *Vinogradov and Jackson* (2015) in natural sandstones.

In electrolytes containing divalent salt ions, the electrolyte pH was lower than the equivalent NaCl electrolyte (see Fig. 6). The lower in magnitude negative zeta potential measured in sandpacks saturated with divalent electrolytes compared with NaCl at ambient temperature, is a result of initially lower pH (Figure 11). Our results are consistent with previous experimental data (*Kosmulski et al*., 2002; *Datta et al*., 2009) who found that addition of divalent cations to NaCl electrolytes of 10.8 mM ionic strength resulted in a more positive zeta potential measured in silica microchannels. *Thanh and Sprik* (2016) also reported smaller in magnitude negative zeta potential in divalent electrolytes compared with NaCl, but their analysis did not extend beyond 1mM.

Datta et al. (2009) concluded that at ambient temperature, the negative zeta potential was smaller in magnitude with addition of Ca^{2+} compared to Mg^{2+}, which agrees with our experimental results (compare black and grey symbols in Figure 5 at 17^{o}C and 23^{o}C). *Datta et al*., (2009) explained their observation (supported by numerical modelling) by a stronger association of Ca^{2+} to the silica surface relative to Mg^{2+}, which led to stronger Van der Waals interactions. They also suggested that smaller hydrated diameter of Ca^{2+} ion compared to the hydrated diameter of Mg^{2+} (the fully hydrated cation diameter reported by *Kielland,* (1937) follows the order: Na (450pm = 4.5Å) → Ca (600pm = 6Å) → Mg (800pm = 8Å)) led to a closer distance of approach to the mineral surface and consequently smaller in magnitude zeta potential.

4.2 Effect of grain size

Zeta potentials measured in the Ottawa sandpacks were generally more negative compared to those measured in Fontainebleau sandpacks regardless of ionic strength and temperature (compare circles with the corresponding triangles in e.g. Fig. 5). As reported in Table 1, the grain size of the Fontainebleau sand is classified as mesh 60 (average grain diameter of 250

μm), while Ottawa sand is mesh 20-30 (grain dimeter between 600 μm and 850 μm). Moreover, the shape of grains for the two sand types is different: Ottawa sand grains are rounded (*Wang et al*., 2015) while the Fontainebleau sand grains are angular (*Montaron and Han*, 2009). We hypothesise that the effective shear plane in Fontainebleau samples is located further away from the mineral surface, thus making the measured apparent zeta potential smaller in magnitude compared with Ottawa samples (see also arguments presented by *AlRoudhan et al*., 2016).

4.3 Implications for CSW

Controlled salinity waterflooding typically involves dilution of the brine injected into oil reservoirs during recovery (*Jackson et al.*, 2016b). Simple dilution from 2M to 0.45M yields no significant change in zeta potential irrespective of temperature if the initial and diluted electrolytes contain Na plus divalent ions or Na ions alone (Fig. 9), consistent with the suggestion of *Vinogradov et al*. (2010) that the diffuse part of the double layer only begins to expand in response to decreasing ionic strength once the double layer thickness exceeds the hydrated radius of the key counter ion(s) (c. 0.45M for Na ions). Dilution of Na electrolyte plus addition of Ca or Mg ions yields a positive change in zeta potential (i.e. the negative zeta potential becomes smaller in magnitude) (Fig. 9); addition of Ca or Mg ions to Na electrolyte at constant ionic strength also yields a positive change in zeta potential and *vice-versa* (Fig. 9). Switching from 2M formation brine (FMB) to 0.45M seawater (SW) also yields no significant change in zeta potential (Fig. 9), consistent with the observation that significant dilution is required to observe improved recovery (often termed a 'low salinity effect' (LSE)) in sandstones. The most significant (negative) change in zeta potential is observed when switching from FMB to dilute (0.015M) SW (SW/30), which involves both dilution and a change in composition (Fig. 9).

If it is assumed that the LSE in sandstones is associated with a negative change in zeta potential (see, for example, *Jackson et al.*, 2016a for a discussion of this assumption), then these results suggest that the most significant LSE will be observed when switching from FMB to dilute seawater in either secondary or tertiary mode, especially if there is a decrease in temperature associated with injection of the dilute seawater. A smaller LSE will be observed at constant high temperature or through selective removal of Ca and Mg at constant ionic strength. No LSE is expected in response to addition of Ca or Mg.

The zeta potential results reported here can be interpreted in terms of the three key mineral-surface-scale mechanisms that may be responsible for improved oil recovery during CSW: double layer expansion (DLE), pH change (ΔpH) and multi-ion exchange (MIE) (*Jackson et al*., 2016b). At high ionic strength, the variation in zeta potential is small and reflects the limited ΔpH that occurs via MIE in response to replacement of Na by Ca or Mg ions. Reduction in ionic strength from 2M to 0.45M yields little or no change in zeta potential as there is no DLE in these concentrated electrolytes (Figure 13; see cluster of points in upper right corner). Further dilution to lower ionic strength (0.015M) yields a change in zeta potential that primarily reflects DLE, although a change in temperature during dilution also results in ΔpH and is associated with MIE. The spread in values of zeta potential at low ionic strength reflects ΔpH and MIE in response to changes in temperature and replacement of Na by Ca or Mg at constant ionic strength (Figure 13; see spread of points across lower left corner). The difference in the temperature sensitivity of Ca and Mg at low ionic strength yields diverging trends when these ions are present.

5. Conclusions

1. In unbuffered experiments on sandpacks the zeta potential is always negative and the behaviour is consistent with natural sandstones investigated previously.

2. At low salinity (<0.45M) the zeta potential decreases in magnitude with increasing temperature, consistent with a decrease in pH.
3. At moderate to high salinity (>0.45M) the zeta potential is independent of temperature within experimental error, consistent with constant pH.
4. There is a difference in the zeta potential response of the sandpacks to Ca and Mg.
   4.1. The zeta potential becomes smaller in magnitude when Ca/Mg are present compared to simple NaCl brine.
   4.2. The zeta potential is smaller in Fontainebleau than Ottawa, with the largest differences observed when Ca/Mg are present.
5. The zeta potential shows a distinct dependence on saturation history: the change in zeta potential relative to NaCl brine is largest for samples that have been exposed to more Ca or Mg.
6. Mg becomes more active than Ca at elevated temperature.
7. For a given ionic strength, temperature and brine composition control pH, which in turn controls zeta potential.
8. The most significant change in zeta potential towards more negative values is observed when samples saturated with high salinity (2M) formation brine are flooded at low temperature with dilute (0.015M) seawater.

6. Acknowledgements

TOTAL are thanked for funding this work and for granting permission to publish.

References:

Afanas'ev, V.N. and A.N. Ustinov (2012). Hydration numbers and the state of water in hydration spheres of magnesium chloride and magnesium sulfate solutions. *Russ. J. Inorg. Chem.*, 57: 1107, doi:10.1134/S0036023612080025.

AlRoudhan, A., Vinogradov, J. and Jackson, M.D. (2016). Zeta Potential of Intact Natural Limestone: Impact of Potential-Determining Ions Ca, Mg and SO_4. *Colloids and Surfaces A: Physicochemical and Engineering Aspects*, Volume 493, Pages 83-98, ISSN 0927-7757, doi:10.1016/j.colsurfa.2015.11.068.

Appelo, C.A.J. (1994), Some Calculations on Multicomponent Transport with Cation Exchange in Aquifers, *Ground Water*, 32: 968–975. doi:10.1111/j.1745-6584.1994.tb00936.x.

Aubert, M. and Q.Y. Atangana, (1996), Self-Potential Method in Hydrogeological Exploration of Volcanic Areas, *Groundwater*, 34: 1010–1016. doi:10.1111/j.1745-6584.1996.tb02166.x.

Bolève, A., F. Janod, A. Revil, A. Lafon, and J.J. Fry (2011). Localization And Quantification Of Leakages In Dams Using Time-Lapse Self-Potential Measurements Associated With Salt Tracer Injection. *Journal of Hydrology*, 403, 242-252, doi:10.1016/j.jhydrol.2011.04.008.

Cissokho, M., H. Bertin, S. Boussour, P. Cordier, and G. Hamon (2010). Low Salinity Oil Recovery on Clayey Sandstone: Experimental Study. *Petrophysics*, 51, 5, 305-313.

Coreño, J., A. Martínez, A. Bolarín, and F. Sánchez (2001), Apatite nucleation on silica surface: A ζ potential approach, *J. Biomed. Mater. Res.*, 57: 119–125. doi:10.1002/1097-4636(200110)57:1<119::AID-JBM1150>3.0.CO;2-P.

Corwin, R.F., and D.B. Hoover (1979). The self-potential method in geothermal exploration, *Geophysics*, 44, Special Section – Geothermal, 226-245, doi:10.1190/1.1440964.

Darnet, M., Maineult, A. and G. Marquis (2004), On the origins of self-potential (SP) anomalies induced by water injections into geothermal reservoirs, *Geophys. Res. Lett*., 31, L19609, doi:10.1029/2004GL020922.

Datta S, Conlisk AT, Li HF, Yoda M. (2009). Effect of Divalent Ions on Electroosmotic Flow in Microchannels, *Mech. Res. Commun*. 36(1), doi:10.1016/j.mechrescom.2008.07.006.

Datta, S., Conlisk, A.T., Kanani, D.M., Zydney, A.L., Fissell, W.H. and S.J. Roy (2010). Characterizating the surface charge of synthetic nano membranes by the streaming potential method, *J. Colloid Interface Sci*., 348(1):85–95, doi:10.1016/j.jcis.2010.04.017.

Delgado, A.V., F. González-Caballero, R.J. Hunter, L.K. Koopal, and J. Lyklema (2007). Measurement and interpretation of electrokinetic phenomena, Journal of Colloid and Interface Science, 309 (2), 194-224, doi:10.1016/j.jcis.2006.12.075.

Fitterman, D.V. and R.F. Corwin (1982), Inversion of self-potential data from the Cerro Prieto geothermal field, Mexico, *Geophysics*, v. 47, p. 938-945, doi:10.1190/1.1441361.

Glover, P. W. J. (2015), Geophysical properties of the near surface Earth: Electrical properties, in *Treatise on Geophysics*, vol. 11, 2nd ed., edited by G. Schubert, pp. 89–137, Elsevier, Oxford.

Glover, P.W.J., E. Walker, and M.D. Jackson (2012). Streaming-potential coefficient of reservoir rock: A theoretical model, *Geophysics*, 77(2), D17-D43, doi:10.1190/geo2011-0364.1.

Gulamali,M. Z., Leinov, E. and M. D. Jackson (2011), Self-potential anomalies induced by water injection into hydrocarbon reservoirs, *Geophysics*, 76, F283–292, doi:10.1190/1.3596010.

Ishido, T., Kikuchi, T. and M. Sugihara, (1989), Mapping Thermally Driven Upflows by the Self-Potential Method, *in Hydrogeological Regimes and Their Subsurface Thermal Effects*

(eds A. E. Beck, G. Garven and L. Stegena), American Geophysical Union, Washington, D. C.. doi:10.1029/GM047p0151.

Ishido, T., Pritchett, J.W., Tosha, T., Nishi, Y. and S. Nakanishi (2013), Monitoring Underground Migration of Sequestered CO2 using Self-potential Methods, *Energy Procedia*, Volume 37, Pages 4077-4084, ISSN 1876-6102, doi:10.1016/j.egypro.2013.06.308.

Jaafar, M.Z., Vinogradov, J., M. D. Jackson (2009). Measurements of Streaming Potential Coupling Coefficient in Sandstones Saturated with High Salinity NaCl Brine. *Geophysical Research Letters* 36, L21306, doi:10.1029/2009GL040549.

Jackson, M.D., Al-Mahrouqi, D. and Vinogradov, J., (2016a), Zeta potential in oil-water-carbonate systems and its impact on oil recovery during controlled salinity water-flooding, *Scientific Reports* 6: 37363, doi:10.1038/srep37363.

Jackson, M.D., Vinogradov, J., Hamon, G. and Chamerois, M. (2016b). Evidence, Mechanisms and Improved Understanding of Controlled Salinity Waterflooding Part 1: Sandstones. *Fuel*, 185, 772-793, ISSN 0016-2361, doi:10.1016/j.fuel.2016.07.075.

Jardani, A., Revil, A. Bolève, A. and J.P. Dupont (2008), Three-dimensional inversion of self-potential data used to constrain the pattern of groundwater flow in geothermal fields, *J. Geophys. Res*., 113, B09204, doi:10.1029/2007JB005302.

Jougnot, D., N. Linde, E.B. Haarder, and M.C. Looms (2015). Monitoring Of Saline Tracer Movement with Vertically Distributed Self-Potential Measurements At The Hobe Agricultural Test Site, Voulund, Denmark, *Journal of Hydrology*, 521, 314-327, doi:10.1016/j.jhydrol.2014.11.041.

Jouniaux, L. and F. Zyserman (2016). A review on electrokinetically induced seismo-electrics, electro-seismics, and seismo-magnetics for Earth sciences, *Solid Earth*, 7, 249-284, doi:10.5194/se-7-249-2016.

Jouniaux, L., and J. P. Pozzi (1995), Streaming potential and permeability of saturated sandstones under triaxial stress: Consequences for electrotelluric anomalies prior to earthquakes, *J. Geophys. Res*., 100(B6), 10,197–10,209, doi:10.1029/95JB00069.

Jouniaux, L., M. L. Bernard, M. Zamora, and J. P. Pozzi, (2000). Streaming potential in volcanic rocks from Mount Pele´e, *J. Geophys. Res*., 105, 8391–8401, doi:10.1029/1999JB900435.

Kielland, J. (1937), Individual Activity Coefficients of Ions in Aqueous Solutions, *J. Am. Chem. Soc*., 59 (9), doi: 10.1021/ja01288a032.

Kosmulski, M., Hartikainen, J., Mączka, E., Janusz, W. and Rosenholm. J.B. (2002). Multiinstrument Study of the Electrophoretic Mobility of Fumed Silica, *Analytical Chemistry*, 74 (1), 253-256, doi:10.1021/ac015584h.

Kuyucak, S. and S-H. Chung (1994). Temperature dependence of conductivity in electrolyte solutions and ionic channels of biological membranes, *Biophysical Chemistry*, 1994, 52 (1), 15-24, doi: 10.1016/0301-4622(94)00034-4.

Leinov, E. and M. D. Jackson (2014). Experimental measurements of the SP response to concentration and temperature gradients in sandstones with application to subsurface geophysical monitoring, *J. Geophys. Res. Solid Earth*, 119, 6855–6876, doi:10.1002/2014JB011249.

Lorne, B., F. Perrier, and J.-P. Avouac (1999), Streaming potential measurements: 1. Properties of the electrical double layer from crushed rock samples, *J. Geophys. Res*., 104(B8), 17857–17877, doi:10.1029/1999JB900156.

MacAllister, D.J., Vinogradov, J., Butler, A.P. and M.D. Jackson (2016). Tidal influence on self-potential measurements. *J. Geophys. Res. Solid Earth,* 121, 8432–8452, doi:10.1002/2016JB013376.

Maineult, A., Y. Bernabé, and P. Ackerer (2004). Electrical Response of Flow, Diffusion, and Advection in a Laboratory Sand Box, *Vadose Zone Journal*, 3 (4): 1180–1192. doi:10.2113/3.4.1180.

Mammen, M., Carbeck, J.D., Simanek, E.E. and G.M. Whitesides (1997). Treating Electrostatic Shielding at the Surface of Silica as Discrete Siloxide·Cation Interactions, *Journal of the American Chemical Society*, 119 (15), 3469-3476, doi:10.1021/ja9638115.

Michel, S., and J. Zlotnicki (1998), Self-potential and magnetic surveying of La Fournaise volcano (Réunion Island): Correlations with faulting, fluid circulation, and eruption, *J. Geophys. Res*., 103(B8), 17845–17857, doi:10.1029/98JB00607.

Millero, F.J., B. DiTrolio, A.F. Suarez, and G. Lando (2009), Spectroscopic measurements of the pH in NaCl brines, *Geochimica et Cosmochimica Acta*, 73(11), 3109-3114, doi:10.1016/j.gca.2009.01.037.

Montaron, B. and M. Han (2009). A connectivity model for the electrical conductivity of sandstone rocks. *SPWLA 50th Annual Logging Symposium*, June 21-24.

Moore, J.R., Glaser, S.D., Morrison, H.F. and G.M. Hoversten (2004), The streaming potential of liquid carbon dioxide in Berea sandstone, *Geophys. Res. Lett*., 31, L17610, doi:10.1029/2004GL020774.

Nelson, P. H. (2005). Permeability, Porosity, and Pore-Throat Size? A Three-Dimensional Perspective, *Petrophysics*, 46 (6), 452–455.

Pierre, A., Lamarche, J.M., Mercier, R., Foissy, A., and J. Persello (1990). Calcium as potential determining ions in aqueous calcite suspensions, *Journal of Dispersion Science and Technology*, 11 (6), 611–635, doi:10.1080/01932699008943286.

Revil, A. and P.A. Pezard, (1998), Streaming electrical potential anomaly along faults in geothermal areas, Geophys. Res. Lett., 25(16), 1944-8007, doi:10.1029/98GL02384.

Revil, A., and H. Mahardika (2013), Coupled hydromechanical and electromagnetic disturbances in unsaturated porous materials, *Water Resour. Res*., 49, doi:10.1002/wrcr.20092.

Revil, A., Finizola, A., Ricci, T., Delcher, E., Peltier, A., Barde-Cabusson, S., Avard, G., Bailly, T., Bennati, L., Byrdina, S., Colonge, J., Di Gangi, F., Douillet, G., Lupi, M., Letort, J. and E. Tsang Hin Sun (2011), Hydrogeology of Stromboli volcano, Aeolian Islands (Italy) from the interpretation of resistivity tomograms, self-potential, soil temperature and soil CO_2 concentration measurements. *Geophysical Journal International*, 186: 1078–1094. doi:10.1111/j.1365-246X.2011.05112.x.

Revil, A., P. A. Pezard, and P. W. J. Glover (1999), Streaming potential in porous media: 1. Theory of the zeta potential, *J. Geophys. Res*., 104(B9), 20,021–20,031, doi:10.1029/1999JB900089.

Saunders, J.H., M.D. Jackson, M.Y. Gulamali, J. Vinogradov, and C.C. Pain (2012), Streaming potentials at hydrocarbon reservoir conditions, *Geophysics*, 77, E77–E90, doi: 10.1190/geo2011-0068.1.

Thanh L.D. and R. Sprik (2016), Zeta potential in porous rocks in contact with monovalent and divalent electrolyte aqueous solutions, *Geophysics*, 81(4), D303-D314, doi: 10.1190/geo2015-0571.1.

Valocchi, A. J., R. L. Street, and P. V. Roberts (1981), Transport of ion-exchanging solutes in groundwater: Chromatographic theory and field simulation, *Water Resour. Res*., 17(5), 1517–1527, doi:10.1029/WR017i005p01517.

Vinogradov, J. and Jackson, M.D. (2015). Zeta potential in Intact Natural Sandstones at Elevated Temperature. *Geophys. Res. Lett*., 42, doi:10.1002/2015GL064795.

Vinogradov, J. and M. D. Jackson (2011). Multiphase streaming potential in sandstones saturated with gas/brine and oil/brine during drainage and imbibition. *Geophys. Res. Lett*., 38, L01301, doi:10.1029/2010GL045726.

Vinogradov, J., Jaafar, M.Z., and M. D. Jackson (2010). Measurement of Streaming Potential Coupling Coefficient in Sandstones Saturated with Natural and Artificial Brines at High Salinity. *J. Geophys. Res*., 115, B12204, doi:10.1029/2010JB007593.

Walker, E., and P.W.J Glover (2018). Measurements of the Relationship Between Microstructure, pH, and the Streaming and Zeta Potentials of Sandstones, *Transp Porous Med*, 121: 183, doi:10.1007/s11242-017-0954-5.

Walker, E., P. W. J. Glover, and J. Ruel (2014). A transient method for measuring the DC streaming potential coefficient of porous and fractured rocks, *J. Geophys. Res. Solid Earth*, 119, 957–970, doi:10.1002/2013JB010579.

Walker, E., P.W.J. Glover, and J. Ruel (2014). A transient method for measuring the DC streaming potential coefficient of porous and fractured rocks, *J. Geophys. Res. Solid Earth*, 119, 957–970, doi:10.1002/2013JB010579.

Wang, S.H., Jiang, J. and M.M. Stack (2015). Methodology Development for Investigation of Slurry Abrasion Corrosion by Integrating an Electrochemical Cell to a Miller Tester, *J Bio Tribo Corros* 1, doi:10.1007/s40735-015-0009-9.

Zavitsas, A. A. (2005). Aqueous Solutions of Calcium Ions: Hydration Numbers and the Effect of Temperature, *J. Phys. Chem. B.* 109 (43), 20636-20640, doi:10.1021/jp053909i.

Figure captions

Figure 1: Experimental setup for measuring the streaming potential. (a) Setup developed by *Vinogradov et al*. [2010], placed in an oven for the elevated temperature measurements of *Vinogradov and Jackson* [2015]. (b) In the new setup, the single core holder is replaced by six core holders with flow driven by a single pump. The core holders and reservoirs are placed in the oven for elevated temperature measurements.

Figure 2: Zeta potential versus ionic strength for simple NaCl brine. Also shown for comparison are previous data for natural sandstones from *Vinogradov et al*. [2010].

Figure 3: Temperature dependence of the zeta potential in Ottawa and Fontainebleau saturated with NaCl electrolyte at (a) low (0.015M) and (b) moderate to high (0.45M and 2M) ionic strength. Also shown for comparison are data from natural sandstones (Stainton, Doddington and St. Bees) published by *Vinogradov and Jackson* [2015], along with the temperature dependence of zeta potential predicted by the models of *Revil et al*. [1999] at low ionic strength and *Saunders et al*. [2012] at high ionic strength. The parameters used in both of the models are identical to those published in *Vinogradov and Jackson* [2015]; the temperature dependence of pH used in both models is taken from the experimental data shown in Figure 4.

Figure 4: Temperature dependence of the effluent pH from Ottawa and Fontainebleau saturated with NaCl electrolyte at (a) low (0.015M) and (b) moderate (0.45M) ionic strength. Also shown for comparison are data from natural sandstones (Stainton, Doddington and St. Bees) published by *Vinogradov and Jackson* [2015], along with data from NaCl electrolytes at similar ionic strength but not in contact with sand or sandstone from *Millero et al*. [2009].

Figure 5: Temperature dependence of the zeta potential in Ottawa and Fontainebleau saturated with $CaCl_2$ and $MgCl_2$ electrolytes at (a) low (0.015M), (b) moderate (0.45M) and (c) high (2M) ionic strength. Also shown for comparison are the equivalent data for NaCl electrolyte from Figure 3.

Figure 6: Temperature dependence of the pH in Ottawa and Fontainebleau saturated with $CaCl_2$ and $MgCl_2$ electrolytes at (a) low (0.015M) and (b) moderate (0.45M) ionic strength. Also shown for comparison are the equivalent data for NaCl electrolyte from Figure 4.

Figure 7: Temperature dependence of the zeta potential in Ottawa and Fontainebleau saturated with pure and mixed $CaCl_2$ electrolytes at (a) low (0.015M) and (b) high (0.45M) ionic strength. The data for pure $CaCl_2$ electrolyte is the same as that shown in Figure 5. Also shown for comparison are the equivalent data for NaCl electrolyte from Figure 3. In experiments where the electrolyte composition changed, the initial composition is shown in brackets (see also Table 3).

Figure 8: Temperature dependence of the zeta potential in Ottawa and Fontainebleau saturated with pure and mixed $MgCl_2$ electrolytes at (a) low (0.015M) and (b) high (0.45M) ionic strength. The data for pure $MgCl_2$ electrolyte is the same as that shown in Figure 5. Also shown for comparison are the equivalent data for NaCl electrolyte

from Figure 3. In experiments where the electrolyte composition changed, the initial composition is shown in brackets (see also Table 3).

Figure 9: Effect of dilution on zeta potential for different electrolyte compositions in (a) Fontainebleau and (b) Ottawa sandpacks. Zeta potential is expressed in terms of the change from the value recorded in the initial (2M) electrolyte. Solid lines denote experiments at 23ºC; dashed lines denote experiments as 120ºC. All zeta potentials recorded were negative. Zeta potentials for 2M NaCl electrolytes at the corresponding temperatures are shown in Fig. 3b. Zeta potentials for 2M FMB are shown in Fig. 10.

Figure 10. Zeta potential as a function of temperature for FMB electrolyte.

Figure 11. The correlation between zeta potential and pH of different electrolytes of (a) low and (b) moderate and high ionic strength. The arrows indicate the increase in temperature and provide trend lines for different electrolytes. The distribution of red and yellow symbols in Fig.12a is a result of varying temperature and differences in grain size and shape between Ottawa and Fontainebleau samples. The spread between the red and yellow trend lines is a result of different activities of Ca (red) and Mg (yellow).

Figure 12. Hysteresis in the temperature dependence of pH in NaCl electrolytes of 0.015M ionic strength.

Figure 13. Summary plot relating changes in zeta potential and electrolyte pH across all of the streaming potential measurements reported here (Figs. 2 – 10) to the key mechanisms thought to be responsible for IOR during LSW (*Jackson et al*., 2016b). Recall that the pH was not varied by addition of acid or base; it varies only in response to changes in electrolyte temperature and/or composition.

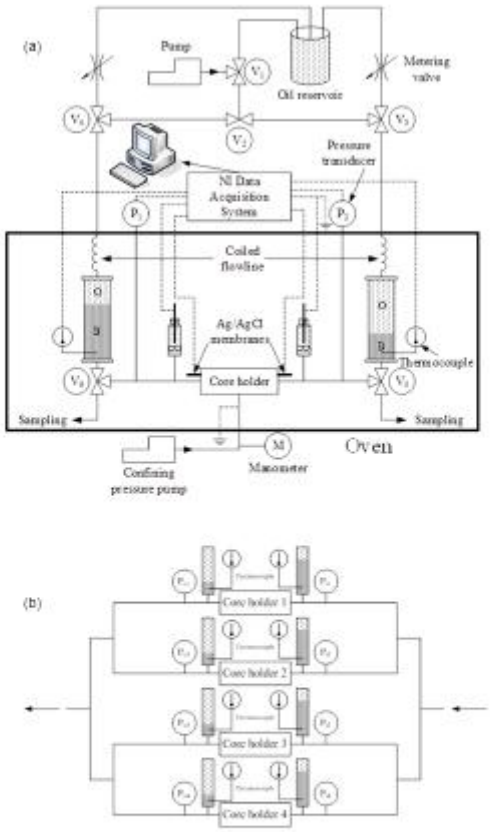

Figure 1

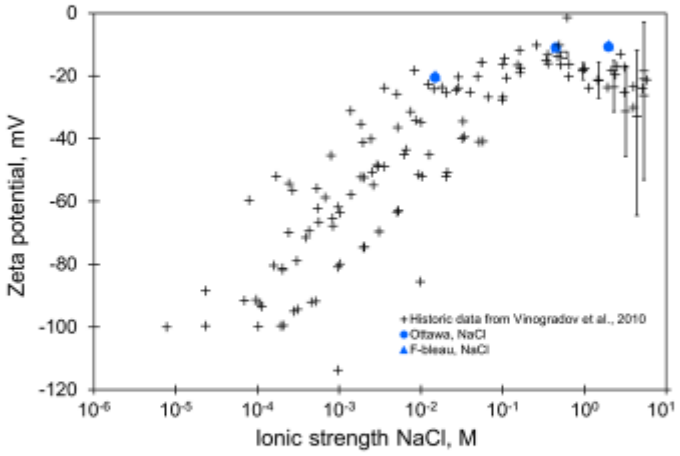

Figure 2

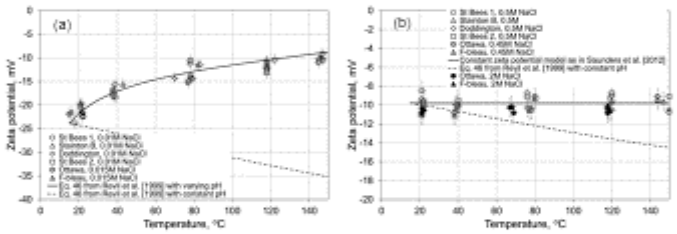

Figure 3

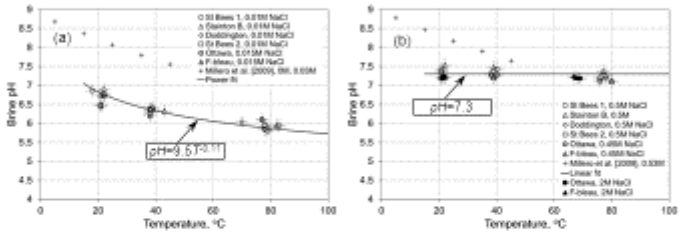

Figure 4

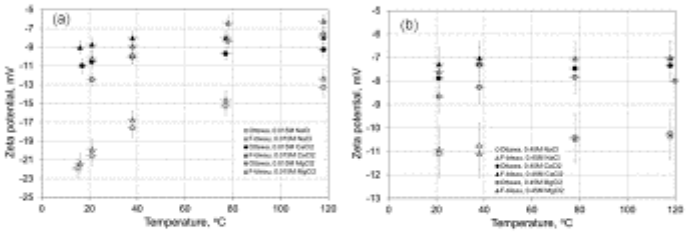

Figure 5

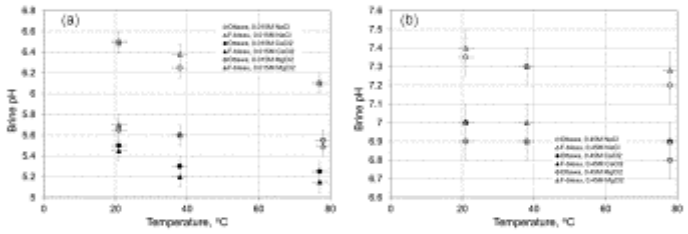

Figure 6

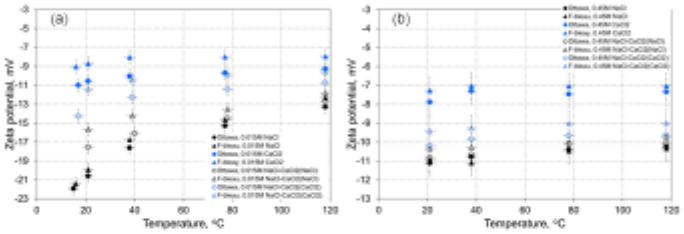

Figure 7

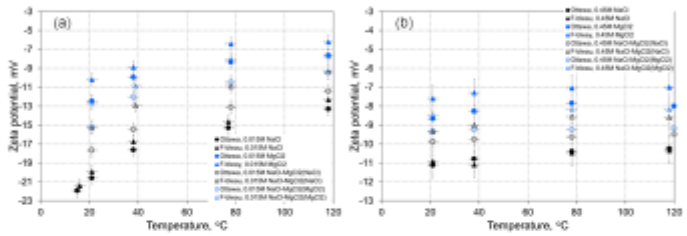

Figure 8

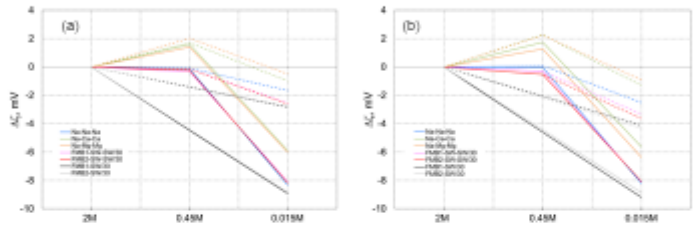

Figure 9

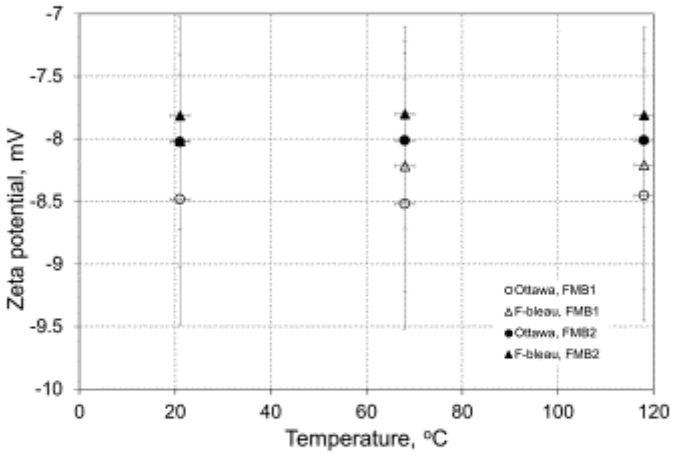

Figure 10

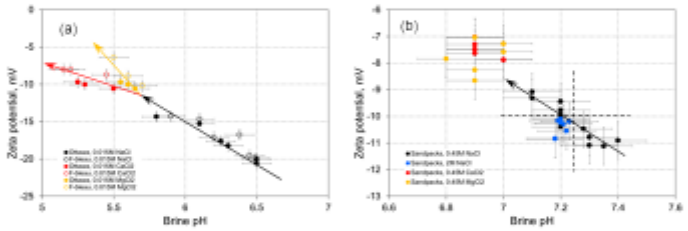

Figure 11

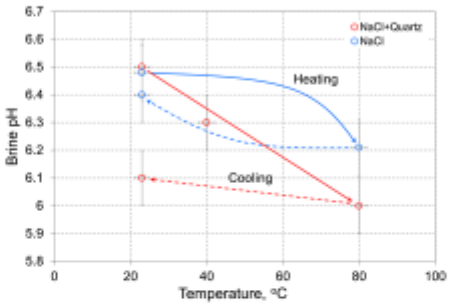

Figure 12

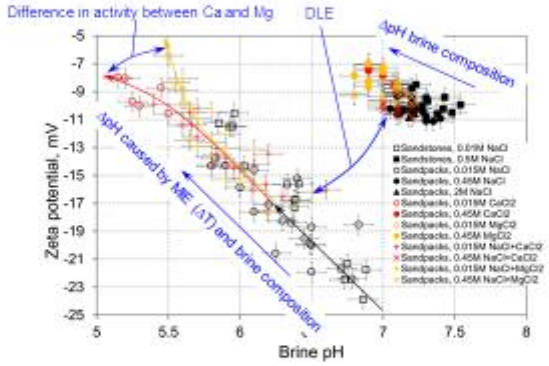

Figure 13

Table 1: Petrophysical properties of sandpacks. Values of the absolute permeability and the intrinsic formation factor include the experimental uncertainty that comprises the inaccuracy of individual measurements and the repeatability of measurements obtained from over 10 sandpacks of each sand type. The absolute permeability was calculated using Darcy's Law from the slope of the linear regression of the flow rate plotted against the pressure difference and using the fluid viscosity as a function of temperature and ionic strength obtained using the approach of *Saunders et al*. (2012). The permeability calculation was performed using at least three different flow rates and after confirming high quality of the regression's linearity ($R^2 > 0.97$).

Sand type	Porosity, %	Permeability, mD	Formation factor, F	Grain size
Ottawa	31±1	2400±100	10±1	20-30 mesh (600 μm – 850 μm)
Fontainebleau	33±1	2200±100	4±0.5	60 mesh (250 μm)

Table 2: Electrolytes and their properties. In the table, '*I*' is the ionic strength, TDS is the Total Dissolved Solids, FMB1 and FMB2 stand for the two artificial formation brines used in the experiments, SW is the seawater and SW/30 represents the 30 times dilution of SW.

Electrolyte ID	*I*, M	Composition	TDS, mg L^{-1}	TDS ratio	Initial pH
NaCl	0.015	NaCl	876.6	N/A	6.5±0.1
NaCl	0.45	NaCl	26298	N/A	7.1±0.2
NaCl	2	NaCl	116880	N/A	7.1±0.2
$CaCl_2$	0.015	$CaCl_2•2H_2O$	714.9	N/A	5.5±0.2
$CaCl_2$	0.45	$CaCl_2•2H_2O$	21447	N/A	6.9±0.2
$MgCl_2$	0.015	$MgCl_2•6H_2O$	956.05	N/A	5.7±0.1
$MgCl_2$	0.45	$MgCl_2•6H_2O$	28681.5	N/A	6.8±0.2
NaCl-$CaCl_2$	0.015	NaCl+$CaCl_2•2H_2O$	828.6	9:1	6.6±0.1
NaCl-$CaCl_2$	0.45	NaCl+$CaCl_2•2H_2O$	24856.9	9:1	7.1±0.2
NaCl-$MgCl_2$	0.015	NaCl+$MgCl_2•6H_2O$	808.57	9:1	6.7±0.2
NaCl-$MgCl_2$	0.45	NaCl+$MgCl_2•6H_2O$	24257	9:1	7.1±0.2
FMB1	2M	NaCl:$CaCl_2$+NaCl:$MgCl_2$	114757.5	9:1 + 14:1	7.1±0.1
FMB2	2M	NaCl:$CaCl_2$+NaCl:$MgCl_2$	99021.5	3:1 + 14:1	6.9±0.1
SW	0.45M	NaCl:$CaCl_2$+NaCl:$MgCl_2$	23330.9	18:1 + 7:1	7.0±0.1
SW/30	0.015M	NaCl:$CaCl_2$+NaCl:$MgCl_2$	777.7	18:1 + 7:1	6.5±0.2

Table 3: Sequence of electrolyte compositions in experiments testing the effect of Ca and Mg concentration on zeta potential in mixed electrolytes.

Electrolyte ID	Initial electrolyte	Initial ionic strength, M	Final electrolyte	Final ionic strength, M

0.015M NaCl-$CaCl_2$ (NaCl)	NaCl	0.015	NaCl-$CaCl_2$ (9:1)	0.015
0.015M NaCl-$CaCl_2$ ($CaCl_2$)	$CaCl_2$	0.015	NaCl-$CaCl_2$ (9:1)	0.015
0.45M $CaCl_2$ (NaCl)	NaCl	0.45	NaCl-$CaCl_2$ (9:1)	0.45
0.45M $CaCl_2$ ($CaCl_2$)	$CaCl_2$	0.45	NaCl-$CaCl_2$ (9:1)	0.45
0.015M NaCl-$MgCl_2$ (NaCl)	NaCl	0.015	NaCl-$MgCl_2$ (9:1)	0.015
0.015M NaCl-$MgCl_2$ ($MgCl_2$)	$MgCl_2$	0.015	NaCl-$MgCl_2$ (9:1)	0.015
0.45M $MgCl_2$ (NaCl)	NaCl	0.45	NaCl-$MgCl_2$ (9:1)	0.45
0.45M $MgCl_2$ ($MgCl_2$)	$MgCl_2$	0.45	NaCl-$MgCl_2$ (9:1)	0.45

Table 4: Sequence of electrolyte compositions in experiments testing the effect of saturation history relevant to CSW on zeta potential. In all cases the initial electrolyte has ionic strength 2M, the second electrolyte (if used) has ionic strength 0.45M, and the third electrolyte has ionic strength 0.015M.

Initial electrolyte (2M)	**Second electrolyte (0.45M)**	**Third electrolyte (0.015M)**
NaCl	NaCl	NaCl
NaCl	$CaCl_2$	$CaCl_2$
NaCl	$MgCl_2$	$MgCl_2$
FMB1	SW	SW/30
FMB2	SW	SW/30
FMB1	-	SW/30
FMB2	-	SW/30

Table 5: Variation of electrolyte pH with temperature for systems in and without contact with silica. The values in bracket correspond to NaCl solutions with no contact with sand.

Electrolyte	Ionic strength, M	T, ^oC	pH	ΔpH from initial
NaCl (w/o sand)	0.015	23	6.5±0.1 (6.5±0.1)	N/A
		40	6.3±0.1 (N/A)	-0.2±0.1 (N/A)
		80	6.0±0.1 (6.2±0.1)	-0.5±0.1 (-0.3±0.1)
		23	6.1±0.1 (6.4±0.1)	-0.4±0.1 (-0.1±0.1)
	0.45	23	7.2±0.2 (7.2±0.2)	N/A
		40	7.1±0.2 (N/A)	-0.1±0.2 (N/A)
		80	7.1±0.2 (7.1±0.2)	-0.1±0.2 (-0.2±0.2)
		23	7.1±0.2 (7.2±0.2)	-0.1±0.2 (0.0±0.2)
	2	23	7.1±0.2 (7.1±0.2)	N/A
		70	6.9±0.2 (6.9±0.2)	-0.2±0.2 (-0.2±0.2)
		23	7.1±0.2 (7.1±0.2)	0.0±0.2 (0.0±0.2)
$CaCl_2$	0.015	23	5.5±0.2	N/A
		40	5.2±0.2	-0.3±0.2
		80	5.2±0.2	-0.3±0.2
		23	5.4±0.2	-0.1±0.2
	0.45	23	6.9±0.2	N/A
		40	6.8±0.2	-0.1±0.2

		80	6.8±0.2	-0.1±0.2
		23	6.9±0.2	0.0±0.2
MgCl2	0.015	23	5.7±0.1	N/A
		40	5.6±0.1	-0.1±0.1
		80	5.5±0.1	-0.2±0.1
		23	5.5±0.1	-0.2±0.1
	0.45	23	7.0±0.2	N/A
		40	7.0±0.2	0.0±0.2
		80	6.9±0.2	-0.1±0.2
		23	7.0±0.2	0.0±0.2
NaCl-$CaCl_2$(NaCl)	0.015	23	6.2±0.1	N/A
		40	6.1±0.1	-0.1±0.1
		80	6.0±0.1	-0.2±0.1
		23	6.1±0.1	-0.1±0.1
	0.45	23	7.1±0.1	N/A
		40	7.0±0.1	-0.1±0.1
		80	7.0±0.1	-0.1±0.1
		23	7.1±0.1	0.0±0.1
NaCl-$CaCl_2$($CaCl_2$)	0.015	23	5.7±0.1	N/A
		40	5.6±0.1	-0.1±0.1
		80	5.5±0.1	-0.2±0.1
		23	5.5±0.1	-0.2±0.1
	0.45	23	7.1±0.1	N/A
		40	7.0±0.1	-0.1±0.1
		80	7.0±0.1	-0.1±0.1
		23	7.1±0.1	0.0±0.1
NaCl-$MgCl_2$(NaCl)	0.015	23	6.1±0.2	N/A
		40	5.9±0.2	-0.2±0.2
		80	5.8±0.2	-0.3±0.2
		23	6.1±0.2	0.0±0.2
	0.45	23	7.2±0.1	N/A
		40	7.1±0.1	-0.1±0.1
		80	7.1±0.1	-0.1±0.1
		23	7.1±0.1	-0.1±0.1
NaCl-$MgCl_2$($MgCl_2$)	0.015	23	5.9±0.1	N/A
		40	5.8±0.1	-0.1±0.1
		80	5.7±0.1	-0.2±0.1
		23	5.7±0.1	-0.2±0.1
	0.45	23	7.0±0.1	N/A
		40	6.9±0.1	-0.1±0.1
		80	6.9±0.1	-0.1±0.1
		23	6.9±0.1	-0.1±0.1